e-Polymers **2003**, no. 051.

http://www.e-polymers.org
ISSN 1618-7229

Organisation and melting of solution grown truncated lozenge polyethylene single crystals

Mingwen Tian [1,2], *Joachim Loos* [1] *

[1] Department of Chemical Engineering and Chemistry, and Dutch Polymer Institute, Eindhoven University of Technology, 5600 MB Eindhoven, The Netherlands; Fax +31-40-243 6999; j.loos@tue.nl

[2] Current address: NT Instruments, Arnhemseweg 34d, 7331 BL Apeldoorn, The Netherlands

(Received: July 21, 2003; published: October 6, 2003)

Abstract: Morphological features and the melting behaviour of truncated lozenge crystals have been studied. For the crystals investigated, the heights of the (110) and the (200) sectors were measured to be 14.5 and 12.7 nm, respectively, using atomic force microscopy (AFM) in contact and non-contact mode. Moreover, melting temperatures of 123°C for the (110) sector and of 120°C for the (200) sector have been measured using real-time AFM during annealing experiments. Applying atomic force acoustic microscopy and the n-alkane decoration technique, no difference in the surface fold organisation of (110) and (200) sectors could be detected. For similar stem lengths, variations in stem tilt angle within the sectors might cause the thickness difference observed. However, a very high tilt angle difference above 20° is required. More likely, a shorter stem length within the (200) sector may cause its lower melting temperature.

Introduction

In order to understand the melting behaviour of polyethylene single crystals, which usually depends on their fold thickness and overall lamellar organisation, an ideal model sample might be the truncated lozenge-shaped crystal due to the possible difference of the fold length or lamellar thickness between the (110) and (200) sectors, as suggested in literature [1,2]. It is generally accepted that when raising the crystallisation temperature, the polymer concentration in solution or the molecular weight, the single crystals formed trend to become truncated in the <100> direction. Truncation in this direction occurs symmetrically giving two additional sectors named as (200) sectors. The morphology and structure of these single crystals have been studied quite extensively [3-5]. Previous studies have suggested that there might be a thickness difference between the (200) and (110) sectors, caused by different stem tilt angles or different surface organisation. However, so far no direct and apparent experimental evidence has confirmed this point.

Moreover, standard differential scanning calorimetry (DSC) has indicated a different thermal behaviour of the two sectors. However, because of the limitations of DSC for the investigation of thermal features related to the initial organisation of the crystals, viz. the reorganisation of the crystals during the heating scan, the data obtained are

rather suggestive [6-9]. In the present part of our study the local melting behaviour of the (110) and (200) sectors will be linked with morphological features and exact local thickness measurements of the crystal.

Results and discussion

Fig. 1a shows the characteristic morphological feature of a truncated lozenge-shaped single crystal after sedimentation on a mica surface: the apparent central pleat oriented along the crystallographic <010> axis, four (110) sectors having some striations along the <310> direction, and two additional (200) sectors having some striations parallel to the <200> folding direction. A schematic representation of the crystal can be found in Fig. 1b.

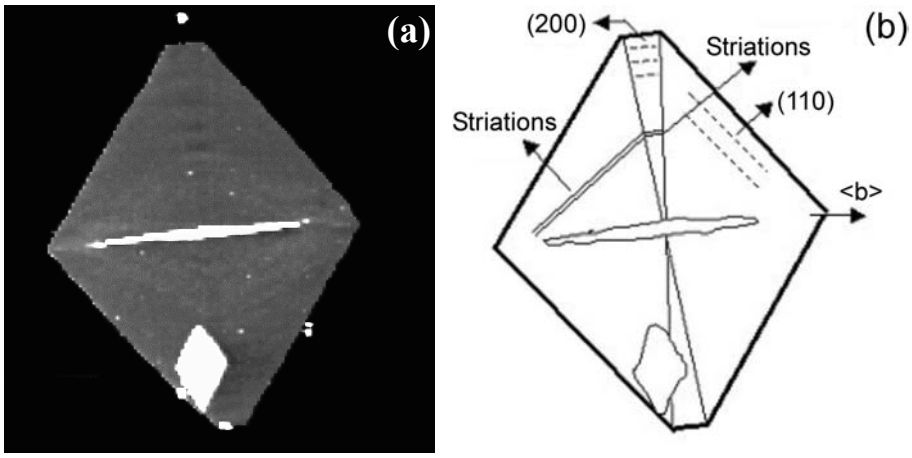

Fig. 1. (a) Height-contrast AFM image of a truncated lozenge-shaped solution grown polyethylene single crystal, and (b) corresponding sketch. Scan size 9 μm × 9 μm; height scale 50 nm

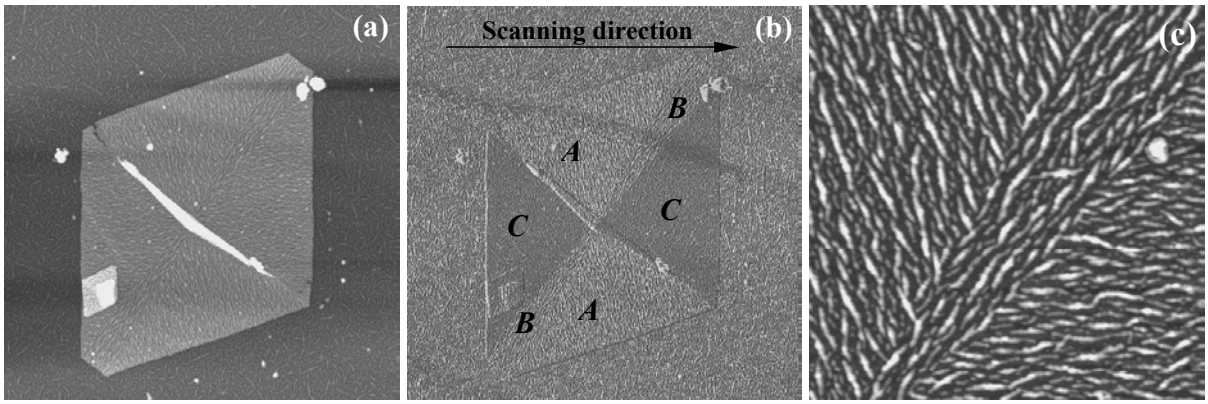

Fig. 2. AFM images recorded on a truncated lozenge PE single crystal after n-alkane decoration: (a) height contrast, (b) phase contrast, and (c) high resolution height contrast images, respectively. Scan size for (a) and (b) is 10 μm × 10 μm, and for (c) 2 μm × 2 μm; height scale is (a) 60 nm and (c) 10 nm; (b) phase shift is 80°

An apparent image of the sectorisation can be obtained using the n-alkane decoration technique. Fig. 2 shows the height and phase contrast AFM images of a truncated lozenge-shaped single crystal after n-alkane decoration. The formed

n-alkane rods are dispersed over the entire sample surface: randomly distributed at the mica and well organised on the crystal surface. On the crystal surface, the n-alkane rods are aligned mainly parallel to the sector growth directions <110> and <200>, respectively. Especially in the high-resolution height contrast image (Fig. 2c) the alignment of the n-alkane rods on the different sectors and the distinct sector boundaries are visible.

Even without n-alkane decoration, high-resolution height contrast AFM images show evidently the sectorisation of truncated lozenge-shaped crystals (Fig. 3). A lamella height of 12.7 nm for the (200) sector and of 14.5 nm for the (110) sector, respectively, can be measured using either non-contact or contact AFM modes (Fig. 3d), which corresponds to a height difference in the order of 1.8 nm. Because AFM height measurements represent the thickness of the crystal and the two chain-folding surfaces, the height difference observed may result from differences of the stem lengths. Alternatively, assuming that both sectors have the same stem length, variations in the stem tilt angle or differences of the fold organisation (e.g., short vs. long loops) may cause the different sector thicknesses.

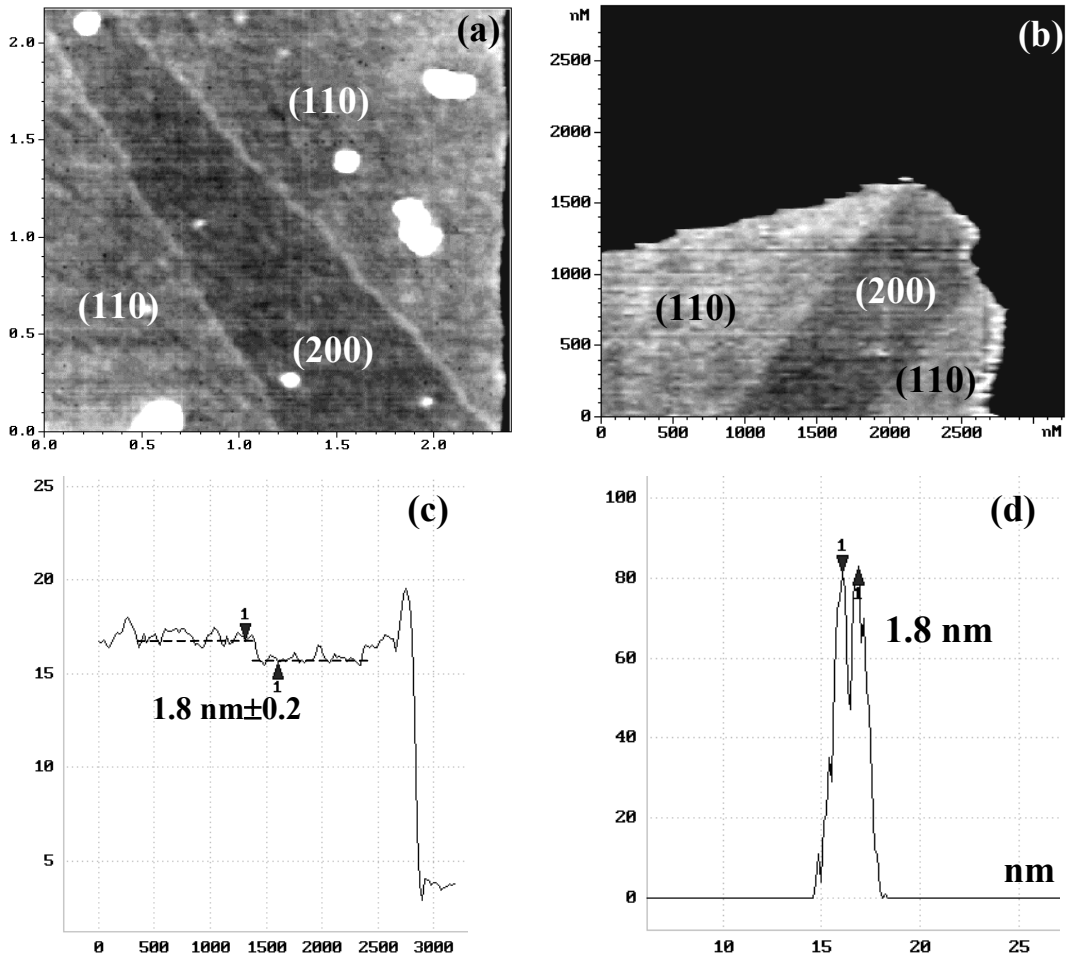

Fig. 3. High-resolution height contrast images of the (110) and (200) sectors of a truncated lozenge-shaped single crystal recorded in (a) non-contact AFM mode (the pronounced sector boundary might be an artefact), and (b) contact AFM mode; (c) corresponding topography line scan crossing the (110) and (200) sectors monitoring a thickness difference of ≈1.8 nm; (d) power spectrum of the dominant height values in Fig. 3b, 12.7 nm for the (200) sector and 14.5 nm for the (110) sector, respectively, and the corresponding height difference of ≈1.8 nm

Apparently, the smoothness of the crystal surface indicates that the thickness difference between the (110) and (200) sectors does not result from differences of the contact behaviour between parts of the crystal and the substrate.

Supposed that the organisation of the fold surfaces results in the thickness difference of the (200) and (110) sectors, whereas the crystal core thickness in the sectors is identical, there should be an elasticity modulus difference between the two sectors. This difference might be detectable using the recently developed dynamic contact AFM mode, the so-called acoustic force atomic microscopy (AFAM). In AFAM mode, the local stiffness of the sample can be calculated from the measured shift of the resonant frequencies of the cantilever. In practice, a fixed excitation frequency is chosen, and at the mean time, the cantilever vibration amplitude or its phase shift is monitored while the sample surface is scanned.

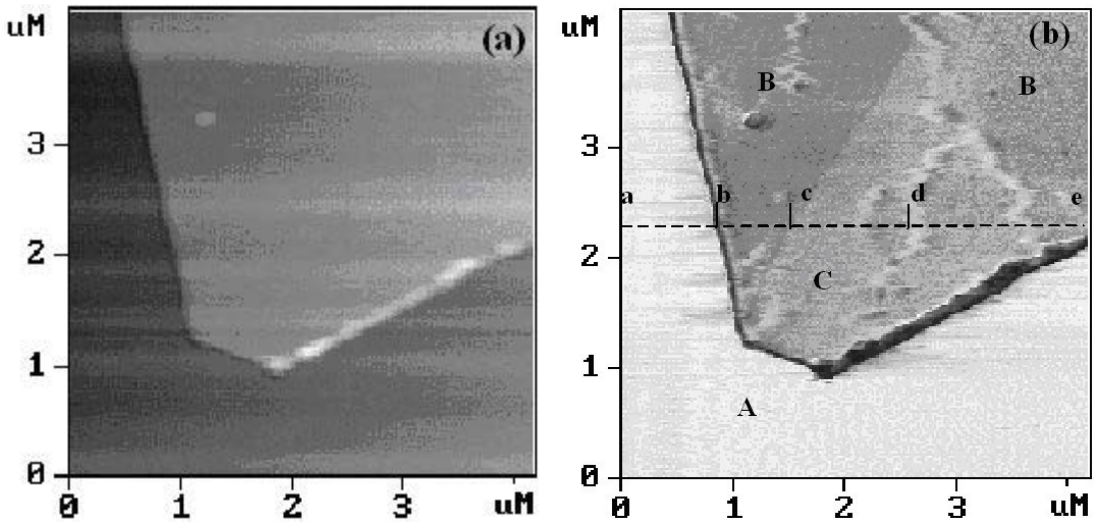

Fig. 4. (a) Height-contrast contact mode AFM image and (b) corresponding AFAM vibration amplitude image for the constant working frequency of ≈ 460 kHz. The mica substrate (A), and the (110) and (200) sectors (B and C), respectively, are visible

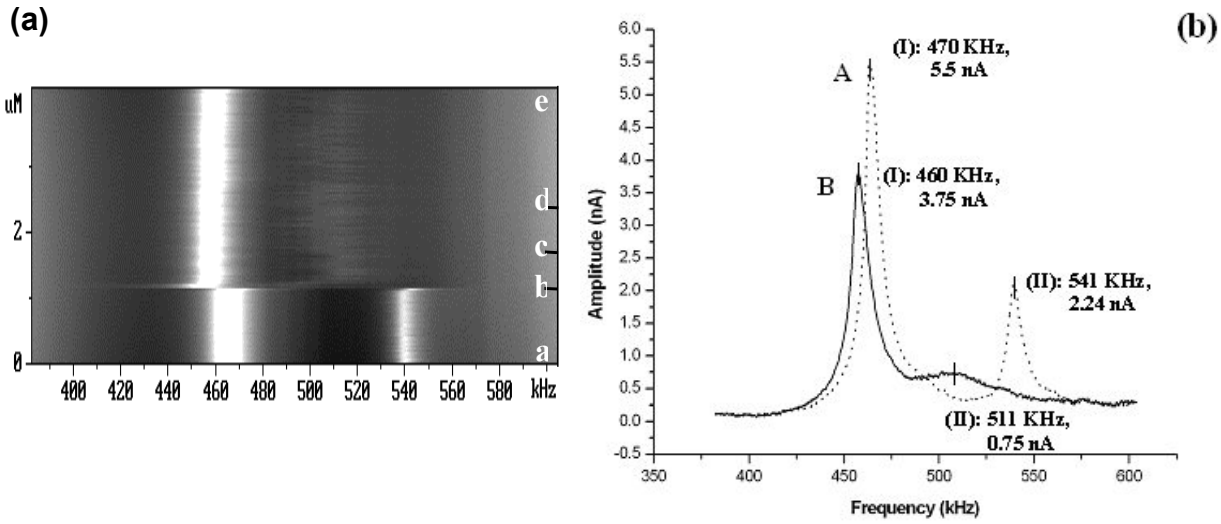

Fig. 5. (a) Amplitude and frequency spectra images recorded along the line as indicated in Fig. 4b, and (b) two characteristic curves of amplitude vs. frequency selected from regions a-b (A) and b-c (B) in Fig. 4b

It is in general accepted that, using a softer cantilever, more sensitivity to recognise surface details can be obtained. In the present case, a rather soft cantilever was used having a resonance frequency of ≈10 kHz and a force constant of ≈ 0.03 N/m. It is evident from Fig. 4 (contact mode AFM, Fig. 4a, and AFAM, Fig. 4b) that besides the damages caused by the interaction of the tip on the single crystal at the edges, there is no apparent difference between the (110) and (200) sectors for the scanning conditions used. Only some features at the sector boundaries can be observed.

The corresponding amplitude and frequency shift image is shown in Fig. 5, which was recorded along the line a-b-c-d-e as indicated in Fig. 4b. In this case, the activation frequency range was set from 380 to 610 kHz. In this image the grey-scale represents the amplitude of the cantilever for a given cantilever frequency, which is changed with the surface stiffness or local micro-elasticity modulus. The image shows obviously the amplitude and frequency variations from the mica region A to the single crystal region B. However, no apparent signal variation is observed between the regions B to C corresponding to the (110) and (200) sectors, respectively. In more detail, Fig. 5b shows two characteristic amplitude vs. frequency curves from region a-b (A) and b-c (B) of Fig. 4b, respectively. Frequency and amplitude of peak I shift from 470 kHz to ≈ 460 kHz and from 5.5 nA to ≈ 3.75nA. Frequency and amplitude of peak II shift from 541 kHz to 511 kHz and from 2.24 nA to ≈ 0.75 nA, respectively. In summary, no noticeable difference of the surface elasticity of the (110) and (200) sectors can be detected, indicating a similar organisation of the fold surfaces of the two sectors.

It is well documented that the chains within a solution grown polyethylene single crystal are tilted. In the case of truncated lozenge crystals, variations of the tilt angles of the (200) and (110) sectors are found, dependent on the crystallisation temperature used. With increasing crystallisation temperature, the tilt angles of the (110) and (200) sectors vary from 14° to 29° and from 18° to 34.5°, respectively [7]. Using

$$L_S = \frac{L}{\cos\theta} \qquad (1)$$

the crystal thickness L for each sector can be calculated. A thickness difference, as measured, of about 2 nm would indicate that for identical crystallisation conditions (it is the same crystal) and for similar stem lengths in both sectors the tilt angle should vary in the order of the maximum observed difference of ≈ 20°, which is very uncertain. Local analysis of the stem tilt angle by means of electron diffraction might provide the necessary information.

In the present study in addition to accurate thickness measurements *ex situ* non-contact AFM annealing experiments of truncated lozenge crystals were performed to measure the melting temperatures of the (110) and (200) sectors. Fig. 6 shows a series of AFM topography images of a truncated lozenge crystal. The images are recorded at room temperature after annealing the crystal at a given temperature for 10 min. At the annealing temperature of 118°C, and somewhat more pronounced for the annealing temperature of 119°C, first morphological changes are observed. Small holes are formed in the (200) sectors, marked by the arrows (Fig. 6a), whereas the two visible (110) sectors remain unaffected. A thick rim surrounds the holes. Further increasing the annealing temperature to 120°C results in full melting of the (200) sector, subsequently followed by recrystallisation of the PE material after cooling down to room temperature (Fig. 6b). In the region of the former (200) sector, melt-crystallised edge-on lamellae are visible. Still, the (110) sectors show no clear

features of reorganisation; only some slight striations in <130> direction (indicated by the arrow) and an overall increase of surface roughness can be observed.

Further increasing the annealing temperature to 122°C, apparent reorganisation of the two (110) sectors can be observed (Fig. 6c, indicated by arrows). Detailed analysis of the annealing and melting behaviour of solution grown polyethylene single crystals is currently in progress and will be presented later. Finally, at an annealing temperature of 123°C the whole single crystal is molten and recrystallised to form lamellae (Fig. 6d).

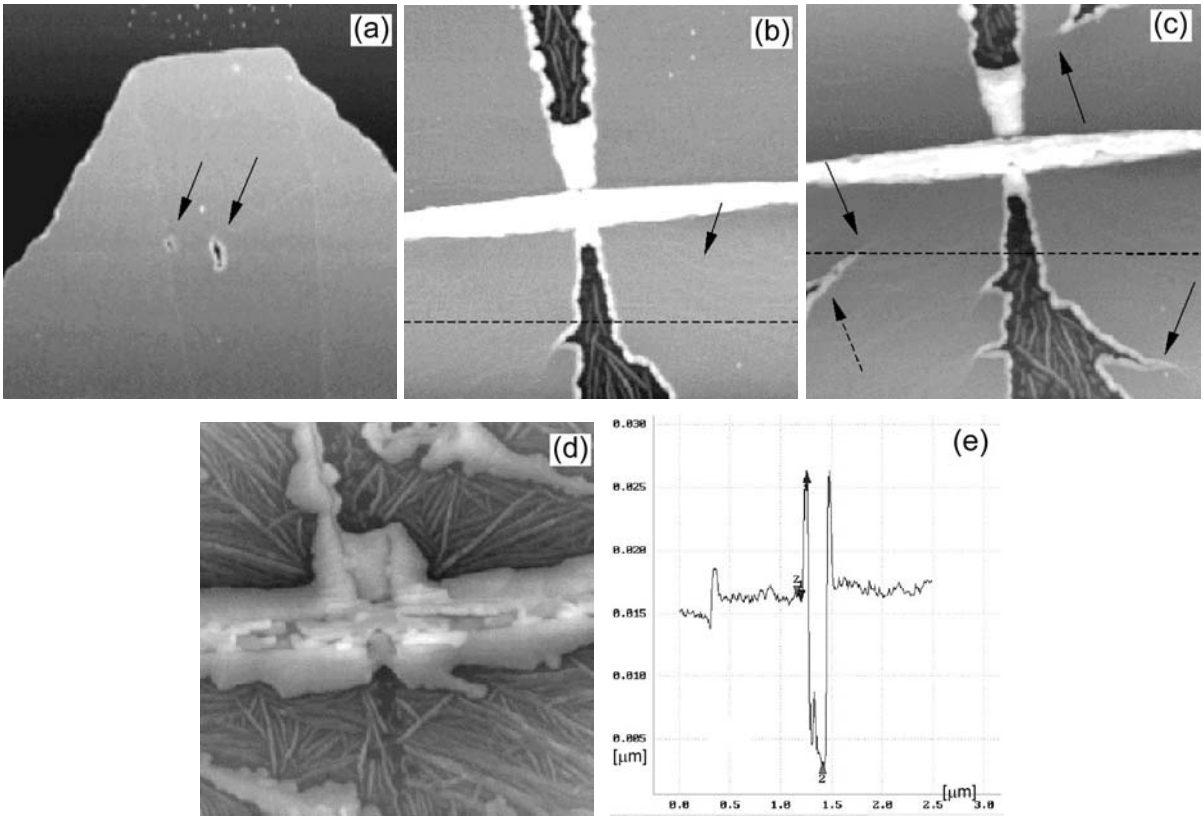

Fig. 6. Series of height-contrast images of an individual single crystal recorded at room temperature after annealing at a temperature of (a) 119°C, (b) 120°C, (c) 122°C and (d) 123°C; the topography line scan (e) corresponds to the line position in Fig. 6c, and is also representative of the line position in Fig. 6b. Scan size 3.0 µm × 3.0 µm for all images; height scale 50 nm

Applying the Gibbs-Thomson equation using the thickness difference observed between the (110) and the (200) sector of 1.8 nm and keeping the surface energy and heat of fusion constant, a melting temperature difference in the order of the 3°C measured can be calculated. However, differences in the stem tilt angle will be present and will cause different surface energies of the (110) and the (200) sectors, which will definitively contribute to the lowering of the melting temperature of the (200) sector in truncated lozenge polyethylene single crystals.

The use of AFM for detailed characterisation of organisation, reorganisation and melting behaviour of solution grown truncated lozenge polyethylene single crystals has resulted in a comprehensive set of data. In the case of crystals grown at a

temperature of 88°C in xylene the thickness difference between the (110) and the (200) sectors has been measured with high accuracy to be 1.8 nm; the (110) and (200) sectors have thicknesses of 14.5 and 12.7 nm, respectively. Beside the thickness difference it has been observed that the (200) sector melts at slightly lower temperatures than the (110) sector of the same single crystal: 120°C in case of (200) and 123°C in case of (110), respectively.

The explanation for this thermal behaviour is that the thermodynamic stability of the (200) sectors is lower because of the shorter stem length within the lamella, which is in accordance with the Gibbs-Thomson formulation. However, different stem tilt angles of the sectors causing variations of the surface energies cannot be neglected. Another possible interpretation of the lower thermodynamic stability of the (200) sector as observed is that the fold organisation of the sectors might be different. TEM observations on the single crystals after n-alkane decoration have shown elsewhere [10] that the rod density of the (200) sectors is lower than that of the (110) sectors; the folding surface of the (200) sectors is more disordered than that of the (110) sectors. However, the presented AFM data related to the n-alkane decoration experiments performed and the AFAM measurements of truncated lozenge single crystals don't show any apparent difference between the two sectors, neither in n-alkane rod density nor in the viscoelastic behaviour of the fold surfaces.

Experimental part

Preparation of solution-grown polyethylene single crystals

For the preparation of truncated lozenge polyethylene (PE) single crystals, the technique of self-seeding was used [11]. A PE/xylene solution was obtained by dissolving PE into the hot solvent at a temperature slightly below its boiling temperature. After pre-crystallisation at 60°C the solution was heated at the seeding temperature T_S = 96°C for 15 - 20 min to form stabilised and uniform nuclei. Subsequently, the solution was transferred to another pre-heated oil bath with the isothermal crystallisation temperature T_C = 88°C. The crystals were removed from the solution by simply dipping freshly cleaved mica in the solution followed by subsequent drying of the samples in a vacuum oven at 40°C for 24 h.

Alkane decoration

Some of the single crystals were decorated with n-alkanes following the route as described by refs. [10,12]. For decoration a linear polyethylene fraction was used having a weight-average molecular weight $M_w \approx 55\,000$ and $M_w/M_n \approx 4.5$. A small piece of this material was placed on an Ω-type wire in the evaporator. A vacuum below $5 \cdot 10^{-5}$ mbar, a voltage of 20 V and a current of 30 A were used to uniformly decompose polyethylene. Moreover, a 15 cm distance between the sample and the wire in the vacuum evaporator was chosen to avoid possible surface melting of the PE single crystals. Using this set-up the resulting n-alkanes condensed on the surface of the single crystal and formed rods by crystallisation. The decoration was performed at room temperature. After decoration - and in the preferred case - the rods were aligned and formed specific patterns, which may reflect the local organisation of the fold surface of the crystal.

Non-contact atomic force microscopy (AFM)

Real-time dynamic AFM investigations of the morphology evolution of PE single crystals were performed using a Smena P47H (NT-MDT Ltd., Moscow, Russia), which is specially designed for scanning force microscopy measurements in a controlled environment, and which is equipped with a hot-stage. The hot-stage is controlled to a temperature stability of better than 0.1°C. The symmetric design of the hot-plate fixation greatly reduces vertical expansion or contraction, leading to a low thermal drift during AFM imaging. The AFM was operated in non-contact mode in air using silicon cantilevers with a spring constant k = 11 - 15 N/m, which were coated with a gold layer for higher laser beam reflectivity. Typical resonance frequencies were 210 - 230 kHz. The AFM has been calibrated using a 25-nm-height standard grating produced by NT-MDT. Ltd., Moscow, Russia. The temperature of the hot stage integrated in the AFM was calibrated using standard test materials, such as azobenzene (T_m = 68°C), acetanilide (T_m = 115°C), phenacetin (T_m = 135°C) and benzanilide (T_m = 163°C). Real-time investigations were performed at real temperature during an annealing experiment.

Contact-mode atomic force acoustic microscopy (AFAM)

Atomic force acoustic microscopy (AFAM), as a member of the dynamic atomic force microscopy modes family, was introduced to discern local elastic data quantitatively by evaluating the cantilever vibration spectra at ultrasonic frequencies. AFAM images can be obtained, in which the contrast depends on the elasticity of the sample surface [13-15].

When the sensor tip is brought to approach a sample surface, the tip-sample interaction modifies the boundary conditions of the vibrating cantilever, leading to some change of resonance frequencies and damping constant, like normal scanning force microscopy. However, the constant resonance vibrations are excited by an ultrasonic transducer, which emits longitudinal acoustic waves into the measured samples. Out-of-plane vibrations of the sample surface are transmitted into the cantilever via the sensor tip. An external frequency generator provides a stable sinusoidal excitation of a piezoelectric transducer coupled to the backside of the sample.

Operating the AFM in the AFAM mode, the frequency for excitation induced by a transducer is selected close to a constant resonance frequency, which depends on the shape of the tip and the local elasticity. When the tip scans the sample surface, a lock-in output signal is fed into an auxiliary channel of the AFM controller, digitised, and displayed as an image. From the obtained AFAM images the stiffness of the local sample area can be calculated from the measured contact resonance frequencies of the cantilever. Gold-coated silicon contact mode cantilevers CSG01 (NT-MDT. Ltd., Moscow, Russia) were used for both conventional contact-mode and AFAM measurements. They have a resonant frequency of 7 - 16 kHz and a force constant of 0.01 - 0.1 N/m; the typical curvature radius is ≈10 nm.

Acknowledgement: We would like to acknowledge the Dutch Polymer Institute (DPI) for support of the presented study. The authors also thank Marcel Dosière, Stephan Hocquet, Bernard Lotz, Jamie Hobbs and Jens-Uwe Sommer, and especially Piet Lemstra and Sanjay Rastogi, for their indefatigable readiness for discussions. Also the support of the people from NT-MDT should be mentioned.

[1] Runt, J.; Harrison, I. R.; Varnell, W. D.; Wang, J. I.; *J. Macromol. Sci., Phys.* **1983**, *B22*, 197.

[2] Bassett, D. C.; Frank, F. C.; Keller, A.; *Nature* **1959**, *184*, 810.

[3] Bassett, D. C.; Frank, F. C.; Keller, A.; *Phil. Mag.* **1963**, *8*, 1753.

[4] Kawai, T.; Keller, A.; *Phil. Mag.* **1965**, *11*, 1165.

[5] Nakagawa, Y.; Toda, A.; Miyaji, H.; *Jpn. J. Appl. Phys.* **1994**, *33*, 3771.

[6] Harrison, I. R.; *J. Macromol. Sci., Chem.* **1974**, *A8*, 43.

[7] Harrison, I. R.; *J. Polym. Sci., Polym. Phys.* **1973**, *11*, 991.

[8] Harrison, I. R.; Runt, J.; *J. Polym. Sci., Polym. Phys.* **1979**, *17*, 321.

[9] Alfonso, G. C.; Ceschia, M.; Chiappa, V.; Pedemonte, E.; *NATO ASI Series, Ser. C: Mathematical and Physical Sciences* **1993**, *405*, 455.

[10] Wittmann, J. C.; Lotz, B.; *J. Polym. Sci., Polym. Phys.* **1985**, *23*, 205.

[11] Blundell, D. J.; Keller, A.; Kovacs, A.; *J. Polym. Sci., Lett.* **1966**, *4*, 487.

[12] Wittmann, J. C.; Lotz, B.; *Makromol. Chem., Rapid. Commun.* **1982**, *3*, 733.

[13] Rabe, U.; Arnold, W.; *Appl. Phys. Lett*. **1994**, *64*, 1493.

[14] Rabe, U.; Janser, K.; Arnold, W.; *Rev. Sci. Instrum.* **1996**, *67*, 3281.

[15] Rabe, U.; Amelio, S.; Kester, E.; Scherer, V.; Hirsekorn, S.; Arnold, W.; *Ultrasonics* **2000**, *38*, 430.